Electronic Supplementary Material (ESI) for Physical Chemistry Chemical Physics.

Supporting Information on "Theoretical and Experimental Examination on SFG Polarization Analysis at Acetonitrile-Water Solution Surfaces"

Kengo Saito,[†] Qiling Peng,[‡] Lin Qiao,[‡] Lin Wang,[†,¶] Tatsuya Joutsuka,[†] Tatsuya Ishiyama,[§] Shen Ye,[*,‡,¶] and Akihiro Morita[*,†,¶]

Department of Chemistry, Graduate School of Science, Tohoku University, Aoba-ku, Sendai 980-8578, Japan, Institute for Catalysis, Hokkaido University, Kita-ku, Sapporo 001-0021, Japan, Elements Strategy Initiative for Catalysts and Batteries (ESICB), Kyoto University, Kyoto 615-8520, Japan, and Department of Applied Chemistry, Graduate School of Science and Engineering, University of Toyama, Toyama 930-8555, Japan

E-mail: ye@cat.hokudai.ac.jp; morita@tohoku.ac.jp

Contents

[*]To whom correspondence should be addressed
[†]Tohoku University
[‡]Hokkaido University
[¶]Kyoto University
[§]University of Toyama

S1 Equilibrium Structure

The equilibrium structure of an isolated acetonitrile molecule was determined by quantum chemical calculation at the level of B3LYP[1,2] with aug-cc-PVTZ basis set[3,4]) using the Gaussian 09 suite.[5] The Cartesian coordinates in the molecule-fixed coordinates system (ξ, η, ζ) are displayed in Table S1. The bond length of $r^0_{\mathrm{CN}} = 1.150$Å, $r^0_{\mathrm{CC}} = 1.453$Å, $r^0_i = 1.089$Å, and the bond angle of $\alpha^0_i = 108.7°$ and $\beta^0_i = 110.2°$.

Table S1: The equilibrium structure of acetonitrile molecule. Unit: Å

site	ξ	η	ζ
N	0.000	0.000	-1.430
C1	0.000	0.000	-0.280
C2	0.000	0.000	1.173
H1	1.022	0.000	1.550
H2	-0.511	-0.885	1.550
H3	-0.511	0.885	1.550

S2 Determining Force Constants

The harmonic force constants in the intramolecular force field of acetonitrile were determined by the following procedure.[6] First, the Hessian $\boldsymbol{H}$ was calculated at the equilibrium structure of acetonitrile (see Table S1) by B3LYP/aug-cc-PVTZ. The obtained Hessian is then converted to the mass-weighted Hessian $\boldsymbol{K}$ by

$$K_{pq} = \frac{1}{\sqrt{m_p m_q}} H_{pq} \tag{S1}$$

where p, q denote the Cartesian degrees of freedom, and m_p, m_q are the masses of the atoms associated to the respective degrees of freedom. $\boldsymbol{K}$ can be diagonalized by a unitary matrix $\boldsymbol{P}$

$$\boldsymbol{P}^\dagger \boldsymbol{K} \boldsymbol{P} = \boldsymbol{\Omega}^2 = \begin{pmatrix} \omega_1^2 & & & \\ & \omega_2^2 & & \\ & & \ddots & \\ & & & \omega_{3N}^2 \end{pmatrix} \tag{S2}$$

ω_i means the i-th harmonic frequency of vibration (including translation and rotation). We substituted the diagonal elements of $\boldsymbol{\Omega}^2$ with the square of the corresponding effective frequencies in Table S2, and the modified diagonal matrix is called $\boldsymbol{\Omega}^2_{\text{eff}}$. The effective frequencies in Table S2 are the experimental ones[7] except for CC stretching, CH_3 symmetric deformation and CN stretching. These three modes are associated to the Fermi resonance of CN stretching, and their frequencies were optimized so as to reproduce the IR and SFG lineshapes of the CN band. The mass-weighted Hessian is modified by back converting $\boldsymbol{\Omega}^2_{\text{eff}}$ as $\boldsymbol{K}_{\text{eff}} = \boldsymbol{P}\boldsymbol{\Omega}^2_{\text{eff}}\boldsymbol{P}^\dagger$, and the Hessian is modified to $\boldsymbol{H}_{\text{eff}}$ accordingly. On the other hand,

Table S2: Effective frequency for fitting.

i	Vib. Modes	Frequency/cm^{-1}
1	CH_3 symm. str.	2954
2	CN str.	2263
3	CH_3 symm. deform.	1369
4	CC str.	909
5,6	CH_3 dissymm. str.	3009
7,8	CH_3 dissymm. deform.	1436
9,10	CH_3 rock.	1041
11,12	CCN linear bend	362

the Hessian is also described with the intramolecular potential model of acetonitrile in Eq. (4) of the main text,

$$H_{\text{model},pq} = \sum_{i,j} k_{ij} \frac{\partial S_i}{\partial x_p} \frac{\partial S_j}{\partial x_q}, \tag{S3}$$

The force constants k_{ij} are determined by the least square fitting so as to minimize the mean square displacement L,

$$L = \sum_{p,q} (H_{\mathrm{model},pq} - H_{\mathrm{eff},pq})^2 \tag{S4}$$

S3 Derivatives of Partial Charge and CRK

The derivatives of partial charge Q and CRK K with respect to the natural internal coordinates S are are calculated by four-point numerical differentiation. The calculated results of $\partial Q_a/\partial S_i$ and $\partial K_{ab}/\partial S_i$ are summarized in Table S3.

S4 Transition Dipole and Polarizability

The derivative of dipole moment ($\partial \mu_p/\partial q_i$) and polarizability tensor ($\partial \alpha_{pq}/\partial q_i$) with respect to the normal mode coordinates are discussed. Here we deal with two vibrational modes, the CN stretching q_2 and CH symmetric stretching q_1. The normal mode coordinates q_i are derived from the transformation matrix $\boldsymbol{P}$ in Eq. (S2), and the displacements in the molecule-fixed Cartesian coordinates are shown in Table S4.

The derivative of dipole moment and polarizability are obtained by four-point numerical differentiation of the quantum chemical calculations by B3LYP/aug-cc-pVTZ along the displacements in Table S4. The results are summarized in Table S5.

Table S5 is utilized to discuss the sign of the hyperpolarizability in the space-fixed coordinates. The hyperpolarizability in the molecule-fixed coordinates, $\beta^{\mathrm{mol}}_{p'q'r'}$, is given as

$$\beta^{\mathrm{mol}}_{p'q'r'} \propto \left(\frac{\partial \alpha_{p'q'}}{\partial q_i}\right)\left(\frac{\partial \mu_{r'}}{\partial q_i}\right) \qquad (i = 1, 2), \tag{S5}$$

where p', q', r' stand for the molecule-fixed coordinates $\xi \sim \zeta$. The subscripts $i = 1$ and 2 mean the CH symmetric stretching and CN stretching modes, respectively. The hyperpolar-

Table S3: Partial differential of partial charges ($\partial Q_a/\partial S_i$) and CRK ($\partial K_{ab}/\partial S_i$) of acetonitrile at its equilibrium geometry. Unit: atomic units.

i		$(\partial Q_a/\partial S_i)$	$(\partial K_{ab}/\partial S_i)$					
			1 (N)	2 (C1)	3 (C2)	4 (H1)	5 (H2)	6 (H3)
1	1	-0.02669	0.09643	-0.23898	-0.31609	0.15288	0.15288	0.15288
	2	0.11780	-0.23898	-0.00556	0.63897	-0.13148	-0.13148	-0.13148
	3	-0.19152	-0.31609	0.63897	-1.15219	0.27644	0.27644	0.27644
	4	0.03347	0.15288	-0.13148	0.27644	0.72508	-0.51146	-0.51146
	5	0.03347	0.15288	-0.13148	0.27644	-0.51146	0.72508	-0.51146
	6	0.03347	0.15288	-0.13148	0.27644	-0.51146	-0.51146	0.72508
2	1	0.31357	0.88622	-1.31122	-0.86022	0.42841	0.42841	0.42841
	2	-0.55095	-1.31122	1.52355	1.11262	-0.44165	-0.44165	-0.44165
	3	0.46463	-0.86022	1.11262	-0.00107	-0.08378	-0.08378	-0.08378
	4	-0.07575	0.42841	-0.44165	-0.08378	-0.62010	0.35856	0.35856
	5	-0.07575	0.42841	-0.44165	-0.08378	0.35856	-0.62010	0.35856
	6	-0.07575	0.42841	-0.44165	-0.08378	0.35856	0.35856	-0.62010
3	1	-0.08061	-0.60468	1.58237	-1.47804	0.16678	0.16678	0.16678
	2	0.08783	1.58237	-4.47143	3.60127	-0.23740	-0.23740	-0.23740
	3	-0.06240	-1.47804	3.60127	0.23997	-0.78773	-0.78773	-0.78773
	4	0.01839	0.16678	-0.23740	-0.78773	1.16450	-0.15307	-0.15307
	5	0.01839	0.16678	-0.23740	-0.78773	-0.15307	1.16450	-0.15307
	6	0.01839	0.16678	-0.23740	-0.78773	-0.15307	-0.15307	1.16450
4	1	0.12760	0.14735	-0.06415	-0.22377	0.04686	0.04686	0.04686
	2	-0.20508	-0.06415	0.94683	0.02577	-0.30282	-0.30282	-0.30282
	3	0.04227	-0.22377	0.02577	-0.36528	0.18776	0.18776	0.18776
	4	0.01174	0.04686	-0.30282	0.18776	-0.19164	0.12992	0.12992
	5	0.01174	0.04686	-0.30282	0.18776	0.12992	-0.19164	0.12992
	6	0.01174	0.04686	-0.30282	0.18776	0.12992	0.12992	-0.19164
5	1	0.00000	0.00000	0.00000	0.00000	0.29078	-0.14539	-0.14539
	2	0.00000	0.00000	0.00000	0.00000	-0.38470	0.19235	0.19235
	3	0.00000	0.00000	0.00000	0.00000	-0.95107	0.47553	0.47553
	4	-0.04932	0.29078	-0.38470	-0.95107	1.44994	-0.20248	-0.20248
	5	0.02466	-0.14539	0.19235	0.47553	-0.20248	-0.72497	0.40495
	6	0.02466	-0.14539	0.19235	0.47553	-0.20248	0.40495	-0.72497
6	1	0.00000	0.00000	0.00000	0.00000	0.00000	0.25183	-0.25183
	2	0.00000	0.00000	0.00000	0.00000	0.00000	-0.33316	0.33316
	3	0.00000	0.00000	0.00000	0.00000	0.00000	-0.82365	0.82365
	4	0.00000	0.00000	0.00000	0.00000	0.00000	-0.35070	0.35070
	5	-0.04271	0.25183	-0.33316	-0.82365	-0.35070	1.25568	0.00000
	6	0.04271	-0.25183	0.33316	0.82365	0.35070	-0.00000	-1.25568

i		$(\partial Q_a/\partial S_i)$	$(\partial K_{ab}/\partial S_i)$					
			1 (N)	2 (C1)	3 (C2)	4 (H1)	5 (H2)	6 (H3)
7	1	0.00000	0.00000	0.00000	0.00000	0.28029	-0.14015	-0.14015
	2	0.00000	0.00000	0.00000	0.00000	-1.02254	0.51127	0.51127
	3	0.00000	0.00000	0.00000	0.00000	2.18245	-1.09123	-1.09123
	4	-0.00100	0.28029	-1.02254	2.18245	-2.55215	0.55597	0.55597
	5	0.00050	-0.14015	0.51127	-1.09123	0.55597	1.27608	-1.11194
	6	0.00050	-0.14015	0.51127	-1.09123	0.55597	-1.11194	1.27608
8	1	0.00000	0.00000	0.00000	0.00000	0.00000	0.24274	-0.24274
	2	0.00000	0.00000	0.00000	0.00000	0.00000	-0.88554	0.88554
	3	0.00000	0.00000	0.00000	0.00000	0.00000	1.89006	-1.89006
	4	0.00000	0.00000	0.00000	0.00000	0.00000	0.96297	-0.96297
	5	-0.00087	0.24274	-0.88554	1.89006	0.96297	-2.21023	0.00000
	6	0.00087	-0.24274	0.88554	-1.89006	-0.96297	0.00000	2.21023
9	1	0.00000	0.00000	0.00000	0.00000	0.47118	-0.23559	-0.23559
	2	0.00000	0.00000	0.00000	0.00000	-1.48132	0.74066	0.74066
	3	0.00000	0.00000	0.00000	0.00000	-4.37058	2.18529	2.18529
	4	0.03523	0.47118	-1.48132	-4.37058	3.62292	0.87890	0.87890
	5	-0.01761	-0.23559	0.74066	2.18529	0.87890	-1.81146	-1.75780
	6	-0.01761	-0.23559	0.74066	2.18529	0.87890	-1.75780	-1.81146
10	1	0.00000	0.00000	0.00000	0.00000	0.00000	0.40805	-0.40805
	2	0.00000	0.00000	0.00000	0.00000	0.00000	-1.28286	1.28286
	3	0.00000	0.00000	0.00000	0.00000	0.00000	-3.78503	3.78503
	4	0.00000	0.00000	0.00000	0.00000	0.00000	1.52230	-1.52230
	5	0.03051	0.40805	-1.28286	-3.78503	1.52230	3.13754	0.00000
	6	-0.03051	-0.40805	1.28286	3.78503	-1.52230	-0.00000	-3.13754
11	1	0.00000	0.00000	0.00000	0.00000	-1.34290	0.67145	0.67145
	2	0.00000	0.00000	0.00000	0.00000	3.71164	-1.85582	-1.85582
	3	0.00000	0.00000	0.00000	0.00000	-3.46294	1.73147	1.73147
	4	0.12702	-1.34290	3.71164	-3.46294	0.73474	0.17973	0.17973
	5	-0.06351	0.67145	-1.85582	1.73147	0.17973	-0.36737	-0.35946
	6	-0.06351	0.67145	-1.85582	1.73147	0.17973	-0.35946	-0.36737
12	1	0.00000	0.00000	0.00000	0.00000	0.00000	-1.16299	1.16299
	2	0.00000	0.00000	0.00000	0.00000	0.00000	3.21438	-3.21438
	3	0.00000	0.00000	0.00000	0.00000	0.00000	-2.99900	2.99900
	4	0.00000	0.00000	0.00000	0.00000	0.00000	0.31130	-0.31130
	5	0.11001	-1.16299	3.21438	-2.99900	0.31130	0.63631	0.00000
	6	-0.11001	1.16299	-3.21438	2.99900	-0.31130	-0.00000	-0.63631

Table S4: The displacements of the normal mode coordinates of CN stretching q_2 and CH symmetric stretching q_1. Unit: atomic units. The equilibrium configuration is given in Table S1, and the reduced mass is set to unity.

(a) CN stretching (2263 cm^{-1})

	ξ	η	ζ
N	0.0	0.0	-1.033×10^{-3}
C1	0.0	0.0	1.521×10^{-3}
C2	0.0	0.0	-1.916×10^{-4}
H1	1.076×10^{-4}	0.0	-3.914×10^{-4}
H2	-5.378×10^{-5}	9.314×10^{-5}	-3.914×10^{-4}
H3	-5.378×10^{-5}	-9.314×10^{-5}	-3.914×10^{-4}

(b) CH symmetric stretching (2954 cm^{-1})

	ξ	η	ζ
N	0.0	0.0	1.491×10^{-5}
C1	0.0	0.0	-2.117×10^{-5}
C2	0.0	0.0	-3.209×10^{-4}
H1	1.247×10^{-2}	0.0	4.433×10^{-3}
H2	-6.234×10^{-3}	-1.080×10^{-2}	4.433×10^{-3}
H3	-6.234×10^{-3}	1.080×10^{-2}	4.433×10^{-3}

izability tensor in the space-fixed coordinates is represented by

$$\beta_{pqr} = \sum_{p'q'r'}^{\xi\sim\zeta} \mathcal{D}_{pp'}\mathcal{D}_{qq'}\mathcal{D}_{rr'}\beta^{\mathrm{mol}}_{p'q'r'}. \tag{S6}$$

Suppose a molecular orientation that the methyl group points toward the positive direction of z axis and the CN head toward the negative direction, that is, $\mathcal{D}$ in Eq. (S6) is nearly a unit tensor. Then Table S5 leads to $\left(\frac{\partial\alpha_{xx}}{\partial q_2}\right)\left(\frac{\partial\mu_z}{\partial q_2}\right) > 0$ for the CN stretching mode, and $\left(\frac{\partial\alpha_{xx}}{\partial q_1}\right)\left(\frac{\partial\mu_z}{\partial q_1}\right) < 0$ for the CH symmetric stretching. These signs are consistent to those of $\mathrm{Im}[\chi^{(2)}_{xxz}] = \mathrm{Im}[\chi^{(2)}_{yyz}]$ in Figures 5 and 6 of the main text, which implies that the acetonitrile molecules tend to point their methyl group toward positive z direction and CN toward negative z direction at the surface.

We also notice in difference in the transition polarizability tensor $(\partial\alpha_{pq}/\partial q_i)$ $(i = 1, 2)$ in Table S5. This tensor is diagonal for both $i = 1$ and 2 due to the C_{3v} symmetry, though the character is fairly different between the two modes. For the CN stretching mode $(i = 2)$ the

Table S5: Partial differential of dipole moment ($\partial\mu_p/\partial q_i$) and polarizability ($\partial\alpha_{pq}/\partial q_i$) at its equilibrium geometry. The equilibrium configuration is given in Table S1, and the normal mode coordinates q_2 and q_1 are in Table S4. Unit: atomic units.

(a) CN stretching

	ξ	η	ζ
$(\partial\mu_p/\partial q_2)$	0.0000	0.0000	0.003275
$(\partial\alpha_{pq}/\partial q_2)$	ξ	η	ζ
ξ	0.02126		
η	0.0000	0.02126	
ζ	0.0000	0.0000	0.1016

(b) CH symmetric stretching

	ξ	η	ζ
$(\partial\mu_p/\partial q_1)$	0.0000	0.0000	-0.005970
$(\partial\alpha_{pq}/\partial q_1)$	ξ	η	ζ
ξ	0.2967		
η	0.0000	0.2967	
ζ	0.0000	0.0000	0.3731

$(pq) = (zz)$ component is dominant, while for the CH symmetric stretching mode ($i = 1$) the tensor is nearly spherical. The nearly spherical character for the CH symmetric stretching mode elucidates the particularly weak SFG signal in the *sps* polarization, discussed in Sec. 4.2 of the main text. While the *sps* signal is associated to β_{yzy} in the space-fixed coordinate, the rotational transformation in Eq. (S6) results in small off-diagonal element of $(\partial\alpha_{yz}/\partial q_1)$ in the space-fixed coordinates.

S5 Details of polarization angle null (PAN) analysis

SFG observation is useful to determine orientation and structures of molecules on a surface or interface. Typically, determination of SFG spectra with at least two polarization combinations of SFG, visible and IR beams, for example, *ssp* (*s*-SFG, *s*-visible and *p*-IR, same as below) and *sps*, are required to carry out these orientation calculations. However, sometimes, SFG spectra under certain polarization combinations are hard to be obtained with reliable resolution in spectral intensity. This makes the orientation analysis difficult or with high risk of errors.

The SFG observation based on a polarization angle null (PAN) analysis has been proposed to conquer the difficulty.[8–14] Generally, SFG intensities (I) under typical polarization

combinations, *ssp*, *sps*, and *ppp*, can be described as,

$$I_{ssp} \propto \left| L_{yy}(\omega_{\mathrm{SFG}}) L_{yy}(\omega_{\mathrm{vis}}) L_{zz}(\omega_{\mathrm{IR}}) \sin\theta_{\mathrm{IR}} \chi^{(2)}_{yyz} \right|^2 I_{\mathrm{vis}} I_{\mathrm{IR}}, \tag{S7a}$$

$$I_{sps} \propto \left| L_{yy}(\omega_{\mathrm{SFG}}) L_{zz}(\omega_{\mathrm{vis}}) L_{yy}(\omega_{\mathrm{IR}}) \sin\theta_{\mathrm{vis}} \chi^{(2)}_{yzy} \right|^2 I_{\mathrm{vis}} I_{\mathrm{IR}}, \tag{S7b}$$

$$\begin{aligned} I_{ppp} \propto \Big| & -L_{xx}(\omega_{\mathrm{SFG}}) L_{xx}(\omega_{\mathrm{vis}}) L_{zz}(\omega_{\mathrm{IR}}) \cos\theta_{\mathrm{SFG}} \cos\theta_{\mathrm{vis}} \sin\theta_{\mathrm{IR}} \chi^{(2)}_{xxz} \\ & - L_{xx}(\omega_{\mathrm{SFG}}) L_{zz}(\omega_{\mathrm{vis}}) L_{xx}(\omega_{\mathrm{IR}}) \cos\theta_{\mathrm{SFG}} \sin\theta_{\mathrm{vis}} \cos\theta_{\mathrm{IR}} \chi^{(2)}_{xzx} \\ & + L_{zz}(\omega_{\mathrm{SFG}}) L_{xx}(\omega_{\mathrm{vis}}) L_{xx}(\omega_{\mathrm{IR}}) \sin\theta_{\mathrm{SFG}} \cos\theta_{\mathrm{vis}} \cos\theta_{\mathrm{IR}} \chi^{(2)}_{zxx} \\ & + L_{zz}(\omega_{\mathrm{SFG}}) L_{zz}(\omega_{\mathrm{vis}}) L_{zz}(\omega_{\mathrm{IR}}) \sin\theta_{\mathrm{SFG}} \sin\theta_{\mathrm{vis}} \sin\theta_{\mathrm{IR}} \chi^{(2)}_{zzz}) \Big|^2 I_{\mathrm{vis}} I_{\mathrm{IR}}, \end{aligned} \tag{S7c}$$

where xz is the incidence plane, xy is the surface plane, θ_{SFG}, θ_{vis}, θ_{IR} are incident (emission) angles for the three beams. L_{xx}, L_{yy} and L_{zz} are the Fresnel coefficients relating the input field to the field in the interfacial layer. The normalized amplitudes can be defined as

$$A_{ssp} \equiv L_{yyz} \sin\theta_{\mathrm{IR}} \chi^{(2)}_{yyz}, \tag{S8a}$$

$$A_{sps} \equiv L_{yzy} \sin\theta_{\mathrm{vis}} \chi^{(2)}_{yzy}, \tag{S8b}$$

$$\begin{aligned} A_{ppp} \equiv & -L_{xxz} \cos\theta_{\mathrm{SFG}} \cos\theta_{\mathrm{vis}} \sin\theta_{\mathrm{IR}} \chi^{(2)}_{xxz} \\ & - L_{xzx} \cos\theta_{\mathrm{SFG}} \sin\theta_{\mathrm{vis}} \cos\theta_{\mathrm{IR}} \chi^{(2)}_{xzx} \\ & + L_{zxx} \sin\theta_{\mathrm{SFG}} \cos\theta_{\mathrm{vis}} \cos\theta_{\mathrm{IR}} \chi^{(2)}_{zxx} \\ & + L_{zzz} \sin\theta_{\mathrm{SFG}} \sin\theta_{\mathrm{vis}} \sin\theta_{\mathrm{IR}} \chi^{(2)}_{zzz}, \end{aligned} \tag{S8c}$$

where the products of Fresnel coefficients are written in simplified form based on a general form as

$$L_{ijk} \equiv L_{ii}(\omega_{\mathrm{SFG}}) L_{jj}(\omega_{\mathrm{vis}}) L_{kk}(\omega_{\mathrm{IR}}). \tag{S9}$$

In the absence of a resonance in visible region, the first two subscripts of the $\chi^{(2)}_{ijk}$ in Eq. (S8c)

Table S6: Related parameters used in the calculation of the PAN analysis at $x_{\mathrm{ACN}} = 0.1$ and 0.2. The refractive indices for SFG were assumed to be same to those of visible.

	Wavelength	n_1	n_2	n'
Visible	800 nm	1.0	$1.329 + 1.25 \times 10^{-7}i$	1.18
IR (C-H)	3300 nm	1.0	$1.45 + 0.0368i$	1.18
IR (C-N)	4500 nm	1.0	$1.33 + 0.0147i$	1.18

are interchangeable, that is, $\chi^{(2)}_{ijk} = \chi^{(2)}_{jik}$. Thus, A_{ppp} can be simplified as

$$\begin{aligned}
A_{ppp} &= -L_{xxz}\cos\theta_{\mathrm{SFG}}\cos\theta_{\mathrm{vis}}\sin\theta_{\mathrm{IR}}\chi^{(2)}_{xxz} \\
&\quad -L_{xzx}\cos\theta_{\mathrm{SFG}}\sin\theta_{\mathrm{vis}}\cos\theta_{\mathrm{IR}}\chi^{(2)}_{xzx} \\
&\quad +L_{zxx}\sin\theta_{\mathrm{SFG}}\cos\theta_{\mathrm{vis}}\cos\theta_{\mathrm{IR}}\chi^{(2)}_{xzx} \\
&\quad +L_{zzz}\sin\theta_{\mathrm{SFG}}\sin\theta_{\mathrm{vis}}\sin\theta_{\mathrm{IR}}\chi^{(2)}_{zzz} \\
&= -L_{xxz}\cos\theta_{\mathrm{SFG}}\cos\theta_{\mathrm{vis}}\sin\theta_{\mathrm{IR}}\chi^{(2)}_{xxz} \\
&\quad \left(-L_{xzx}\cos\theta_{\mathrm{SFG}}\sin\theta_{\mathrm{vis}}\cos\theta_{\mathrm{IR}} + L_{zxx}\sin\theta_{\mathrm{SFG}}\cos\theta_{\mathrm{vis}}\cos\theta_{\mathrm{IR}}\right)\chi^{(2)}_{xzx} \\
&\quad +L_{zzz}\sin\theta_{\mathrm{SFG}}\sin\theta_{\mathrm{vis}}\sin\theta_{\mathrm{IR}}\chi^{(2)}_{zzz} \qquad \text{(S10)}
\end{aligned}$$

As pointed out by Shultz *et al.*, two coefficients for $\chi^{(2)}_{xzx}$ in the above equation are cancelled out each other if the incident angles of visible and IR beams are identical.[14] In fact, we found that the sum of the two coefficients is close to zero even the two angles are not exactly the same.

Figure S1 shows calculation results on the acetonitrile surface for the four coefficients in Eq. (S10) as a function of incident angle of visible beam ($\lambda = 800$ nm) while that of IR ($\lambda = 3300$ nm) is fixed at 50 degree. Other parameters used in the estimate of the Fresnel coefficients are summarized in Table S6. In Figure S1, the sum of term 2 (blue trace) and 3 (black trace) is shown as a trace in a color of cyan. The value of the sum (cyan trace) drops to zero when the incident angel of the visible angle is equal to that of IR beam (50 degree) and keeps to be very small with further increase of incident angel of visible. At visible angle at 70 degree which is typically used in our experiments, the second and three

Figure S1: Calculated Fresnel coefficients for *ppp*-polarization combination as a function of incident angle of visible light. The red, blue, black and green traces correspond to the first, second, third and fourth terms in Eq. (S10). The dotted line with cyan color corresponds the sum of the second and the third terms. The incident angle of the IR beam is fixed at 50°. See text for details.

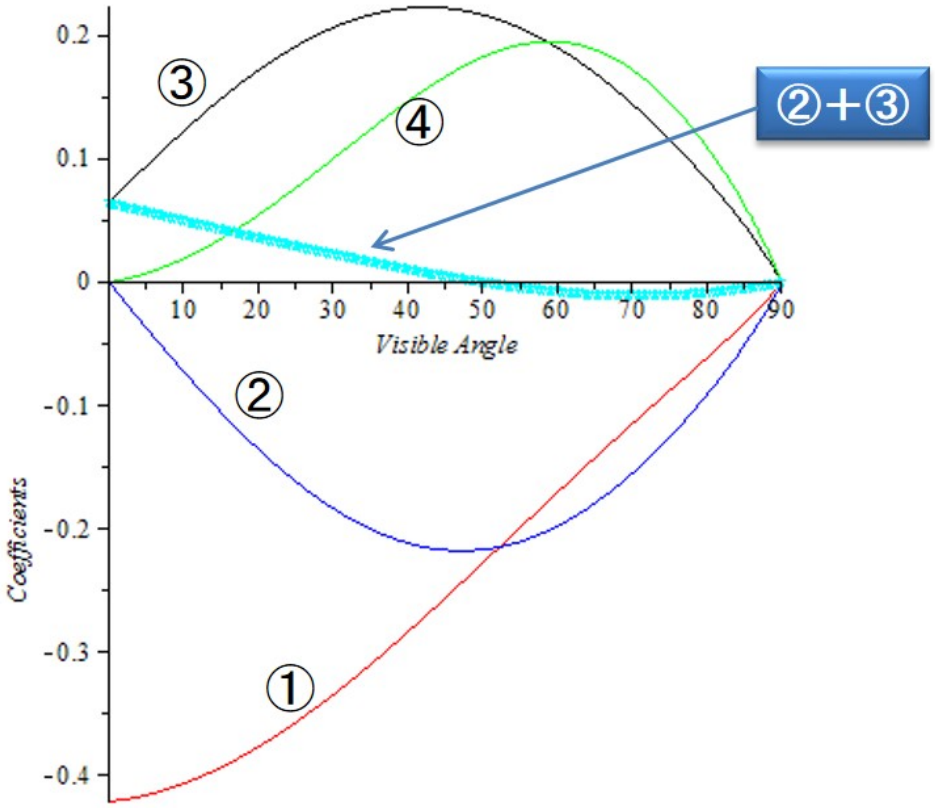

terms are −0.155 and 0.144. The difference (−0.011) is only *ca.* 5 % of the original values. The two terms in Eq. (S10) may be ignored under the approximation. Thus, A_{ppp} can be further simplified as

$$\begin{aligned} A_{ppp} \simeq & -L_{xxz}\cos\theta_{\mathrm{SFG}}\cos\theta_{\mathrm{vis}}\sin\theta_{\mathrm{IR}}\chi^{(2)}_{xxz} \\ & +L_{zzz}\sin\theta_{\mathrm{SFG}}\sin\theta_{\mathrm{vis}}\sin\theta_{\mathrm{IR}}\chi^{(2)}_{zzz}. \end{aligned} \tag{S11}$$

Based on the experimental method proposed, the PAN is collected by linearly polarizing the visible at an angle Ω_{vis}, for example, ±45 degree (facing along the beam propagating

direction, counterclockwise rotation is positive) and IR at p-polarization (0 degree). Then, the SFG at polarization angle of Ω_{SFG} will be

$$A_{\Theta\Omega p} = \cos\Theta_{\mathrm{SFG}} \cos\Omega_{\mathrm{vis}} A_{ppp} \pm \sin\Theta_{\mathrm{SFG}} \sin\Omega_{\mathrm{vis}} A_{ssp} \tag{S12}$$

As $\Theta_{\mathrm{SFG}} = 0^\circ$ or 180°, SFG is p-polarized; as $\Theta_{\mathrm{SFG}} = 90^\circ$ or 270°, SFG is s-polarized. If $\Omega_{\mathrm{vis}} = \pm 45^\circ$, we can change the form as follows,

$$\begin{aligned} A_{\Theta\pm 45^\circ p} &= \frac{1}{\sqrt{2}} \left\{ \cos\Theta_{\mathrm{SFG}} \left(-L_{xxz} \cos\theta_{\mathrm{SFG}} \cos\theta_{\mathrm{vis}} \sin\theta_{\mathrm{IR}} \chi^{(2)}_{xxz} + L_{zzz} \sin\theta_{\mathrm{SFG}} \sin\theta_{\mathrm{vis}} \sin\theta_{\mathrm{IR}} \chi^{(2)}_{zzz} \right) \right. \\ &\qquad \left. \pm \sin\Theta_{\mathrm{SFG}} L_{yyz} \sin\theta_{\mathrm{IR}} \chi^{(2)}_{xxz} \right\} \\ &= \frac{1}{\sqrt{2}} \left\{ \left(-\cos\Theta_{\mathrm{SFG}} L_{xxz} \cos\theta_{\mathrm{SFG}} \cos\theta_{\mathrm{vis}} \pm \sin\Theta_{\mathrm{SFG}} L_{yyz} \right) \chi^{(2)}_{xxz} \right. \\ &\qquad \left. + \cos\Theta_{\mathrm{SFG}} L_{zzz} \sin\theta_{\mathrm{SFG}} \sin\theta_{\mathrm{vis}} \chi^{(2)}_{zzz} \right\} \sin\theta_{\mathrm{IR}}. \end{aligned} \tag{S13}$$

If $\Theta_{\mathrm{SFG}} = \pm 90^\circ$, Eq. (S12) changes to

$$A_{\Theta\pm 45^\circ p} = \frac{1}{\sqrt{2}} \left\{ \pm L_{yyz} \sin\theta_{\mathrm{IR}} \chi^{(2)}_{xxz} \right\}, \tag{S14}$$

i.e., SFG intensity under this condition will only depend on $\chi^{(2)}_{xxz}$. On the other hand, $\chi^{(2)}_{xxz}$ will not contribute to the SFG signal in Eq. (S13) at the SFG polarization angle Θ_{SFG} satisfying the following condition,

$$\tan\Theta_{\mathrm{SFG}} = \pm \cos\theta_{\mathrm{SFG}} \cos\theta_{\mathrm{vis}} \frac{L_{xxz}}{L_{yyz}}. \tag{S15}$$

The SFG signal of Eq. (S13) vanishes at the following SFG polarization angle $\Theta_{\mathrm{SFG}} = \Theta_{\mathrm{null}}$, *i.e.*

$$\left(-\cos\Theta_{\mathrm{null}} L_{xxz} \cos\theta_{\mathrm{SFG}} \cos\theta_{\mathrm{vis}} \pm \sin\Theta_{\mathrm{null}} L_{yyz} \right) \chi^{(2)}_{xxz} + \cos\Theta_{\mathrm{null}} L_{zzz} \sin\theta_{\mathrm{SFG}} \sin\theta_{\mathrm{vis}} \chi^{(2)}_{zzz} = 0.$$

Therefore,

$$\begin{aligned}\frac{\chi^{(2)}_{zzz}}{\chi^{(2)}_{xxz}} &= \frac{\cos\Theta_{\text{null}} L_{xxz}\cos\theta_{\text{SFG}}\cos\theta_{\text{vis}}}{\cos\Theta_{\text{null}} L_{zzz}\sin\theta_{\text{SFG}}\sin\theta_{\text{vis}}} \mp \frac{\sin\Theta_{\text{null}} L_{yyz}}{\cos\Theta_{\text{null}} L_{zzz}\sin\theta_{\text{SFG}}\sin\theta_{\text{vis}}} \\ &= \frac{L_{xxz}\cos\theta_{\text{SFG}}\cos\theta_{\text{vis}}}{L_{zzz}\sin\theta_{\text{SFG}}\sin\theta_{\text{vis}}} \mp \frac{\tan\Theta_{\text{null}} L_{yyz}}{L_{zzz}\sin\theta_{\text{SFG}}\sin\theta_{\text{vis}}} \\ &= \frac{L_{xxz}\cos\theta_{\text{SFG}}\cos\theta_{\text{vis}} \mp \tan\Theta_{\text{null}} L_{yyz}}{L_{zzz}\sin\theta_{\text{SFG}}\sin\theta_{\text{vis}}}. \end{aligned} \tag{S16}$$

If we are able to determine the null angle Θ_{null}, we are able to determine the ratio between $\chi^{(2)}_{zzz}$ and $\chi^{(2)}_{xxz}$ since other parameters in the equation are constants for the optical setup and can be calculated. Then, we are able to estimate the orientation angle based on the ratio.

In the present experiment, the polarization of visible beam was fixed at -45 degree. Therefore, the final equation to derive the $\chi^{(2)}$ ratio is given by

$$\frac{\chi^{(2)}_{zzz}}{\chi^{(2)}_{xxz}} = \frac{L_{xxz}\cos\theta_{\text{SFG}}\cos\theta_{\text{vis}} + \tan\Theta_{\text{null}} L_{yyz}}{L_{zzz}\sin\theta_{\text{SFG}}\sin\theta_{\text{vis}}}. \tag{S17}$$

In fact, when the experimental conditions are kept constant, $A_{\Theta\pm45^\circ p}$ in Eq. (S13) can be simplified as a function of polarization angle of SFG,

$$A_{\Theta\pm45^\circ p} = a\sin\left(\Theta_{\text{SFG}} - \Theta_0\right), \tag{S18}$$

where a is a constant, only depending on the physical properties and optical conditions of the system. Θ_0 is an angle at which the observed SFG intensity (proportional to $|A_{\Theta\pm45^\circ p}|^2$) becomes zero. *i.e.*, null angle, Θ_{null}. By this way, the normalized SFG peak intensity can be expressed as a function of $\sin^2\Theta_{\text{SFG}}$ as

$$I_{\text{SFG}} = a^2\sin^2\left(\Theta_{\text{SFG}} - \Theta_{\text{null}}\right). \tag{S19}$$

Θ_{null} can be determined by fitting the experimental results using Eq. (S19).

S6 Anisotropy of Raman Tensor

We have argued the failure of the bond polarizability model to describe the anisotropy of Raman tensor R in Sec. 5.3.1 of the main text. The R parameter for the methyl symmetric CH stretching vibration of acetonitrile is smaller than 1, while the bond polarizability model predicts a value larger than 1. We discuss this issue in relation to other molecules.

Table S7 shows the calculated Raman tensor and its anisotropy of CH_3X molecules having the C_{3v} symmetry, where R is defined using the natural internal coordinate S_1 for the methyl symmetric CH stretching, $S_1 = (\Delta r_1 + \Delta r_2 + \Delta r_3)/\sqrt{3}$ (see Eq. (2) of the main text), by

$$R = \frac{(\partial \alpha_{\xi\xi}/\partial S_1)}{(\partial \alpha_{\zeta\zeta}/\partial S_1)}. \tag{S20}$$

$R > 1$ is observed for methane (CH_4), ethane (CH_3CH_3) and CH_3F, whereas $R < 1$ for CH_3Br and CH_3CN. The above results suggest that electronically soft moieties tend to reduce the R values. The reduced R values for the latter molecules are mainly attributed to the enhancement of the $(\partial \alpha_{\zeta\zeta}/\partial S_1)$ element.

Figure S2 displays orbital energies as a function of S_1. The orbital energies of CH σ and σ^* are quite similar among these CH_3X molecules. The orbital energies of CH σ and σ^* are strongly influenced by the S_1 coordinate, and the energy gap decreases with increasing S_1 (CH bond). On the other hand, the other orbital energies are nearly invariant over the S_1 coordinate. Comparing the energy levels of various molecules, remarkable difference is seen in the LUMO energy. In CH_3CN molecule, the LUMO energy is significantly lower than that of CH_3F. This is indicative of the hyperconjugation between the CH σ and the CN π^* (LUMO).

Table S7: Calculated Raman tensor and its anisotropy in CH_3X molecules by B3LYP/aug-cc-pVTZ. Unit: atomic units.

	$(\partial\alpha_{\xi\xi}/\partial S_1)$	$(\partial\alpha_{\zeta\zeta}/\partial S_1)$	R
CH_3H	0.367	0.174	2.11
CH_3CH_3[(a)]	0.328	0.272	1.21
CH_3F	0.349	0.197	1.77
CH_3Cl	0.288	0.306	0.942
CH_3Br	0.268	0.342	0.786
CH_3CN	0.296	0.370	0.798[(b)]

[(a)]staggered ethane. [(b)]small difference from $R = 0.78$ in the main text comes from the difference in normal mode coordinate ν_1 and the natural internal coordinate S_1.

Figure S2: Orbital energy levels as a function of S_1. Green solid and dotted lines denote CH σ and σ^*. Red and blue lines denotes LUMO and HOMO, respectively. Unit: atomic units.

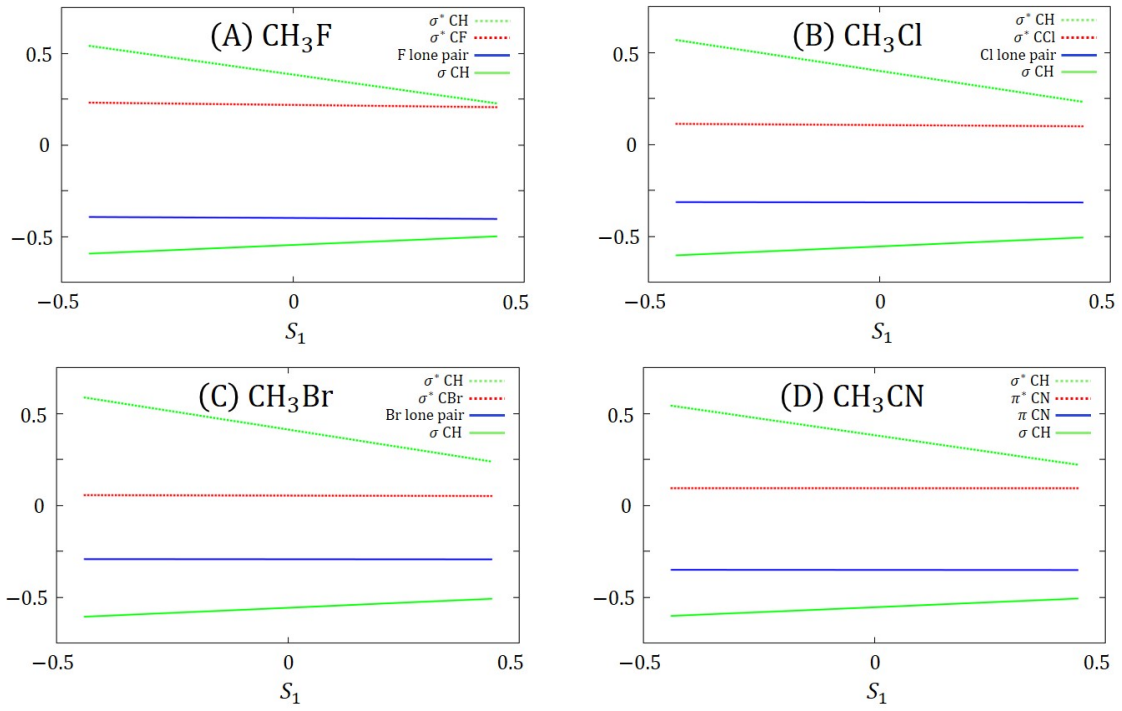

References

(1) Becke, A. D. *J. Chem. Phys.* **1993**, *98*, 5648–5652.

(2) Lee, C.; Yang, W.; Parr, R. G. *Phys. Rev. B* **1988**, *37*, 785–789.

(3) Dunning, Jr., T. H. *J. Chem. Phys.* **1989**, *90*, 1007–1023.

(4) Kendall, R. A.; Dunning, Jr., T. H.; Harrison, R. J. *J. Chem. Phys.* **1992**, *96*, 6796–6806.

(5) Frisch, M. J. et al. *Gaussian 09, revision C.01*; Gaussian, Inc.: Wallingford CT, 2010.

(6) Kawaguchi, T.; Shiratori, K.; Henmi, Y.; Ishiyama, T.; Morita, A. *J. Phys. Chem. C* **2012**,

(7) NIST Chemistry WebBook. http://webbook.nist.gov/chemistry/.

(8) Heinz, T. F.; Tom, H. W. K.; Shen, Y. R. *Phys. Rev. A* **1983**, *28*, 1883–1885.

(9) Zhang, T. G.; Zhang, C. H.; Wong, G. K. *J. Opt. Soc. Am. B* **1990**, *7*, 902–907.

(10) Lü, R.; Gan, W.; Wang, H. *Chin. Sci. Bull.* **2003**, *48*, 2183–2187.

(11) Gan, W.; hua Wu, B.; Chen, H.; Guo, Y.; fei Wang, H. *Chem. Phys. Lett.* **2005**, *406*, 467–473.

(12) Wang, H. F.; Gan, W.; Lu, R.; Rao, Y.; Wu, B. H. *Int. Rev. Phys. Chem.* **2005**, *24*, 191–256.

(13) Groenzin, H.; Li, I.; Shultz, M. J. *J. Chem. Phys.* **2008**, *128*, 214510.

(14) Shultz, M. J.; Bisson, P.; Groenzin, H.; Li, I. *J. Chem. Phys.* **2010**, *133*, 054702.